International Journal of Nanomedicine

Dovepress
open access to scientific and medical research

Open Access Full Text Article

ORIGINAL RESEARCH

Silver-Containing Titanium Dioxide Nanocapsules for Combating Multidrug-Resistant Bacteria

This article was published in the following Dove Press journal:
International Journal of Nanomedicine

Nelly Hérault[1,*]
Julia Wagner[2–4,*]
Sarah-Luise Abram[1]
Jérôme Widmer[2]
Lenke Horvath[1]
Dimitri Vanhecke[5]
Carole Bourquin[2–4,*]
Katharina M Fromm[1,*]

[1]Department of Chemistry, University of Fribourg, Fribourg 1700, Switzerland; [2]Department of Medicine, University of Fribourg, Fribourg 1700, Switzerland; [3]Institute of Pharmaceutical Sciences of Western Switzerland, University of Geneva, Geneva 1211, Switzerland; [4]Department of Anaesthesiology, Pharmacology, Intensive Care and Emergency Medicine, Faculty of Medicine, University of Geneva, Geneva 1211, Switzerland; [5]Adolphe Merkle Institute, University of Fribourg, Fribourg 1700, Switzerland

*These authors contributed equally to this work

Background: Joint arthroplasty has improved the quality of life of patients worldwide, but infections of the prosthesis are frequent and cause significant morbidity. Antimicrobial coatings for implants promise to prevent these infections.

Methods: We have synthesized nanocapsules of titanium dioxide in amorphous or anatase form containing silver as antibacterial agent and tested their impact on bacterial growth. Furthermore, we explored the possible effect of the nanocapsules on the immune system. First, we studied their uptake into macrophages using a combination of electron microscopy and energy-dispersive spectroscopy. Second, we exposed immune cells to the nanocapsules and checked their activation state by flow cytometry and enzyme-linked immunosorbent assay.

Results: Silver-containing titanium dioxide nanocapsules show strong antimicrobial activity against both *E. coli* and *S. aureus* and even against a multidrug-resistant strain of *S. aureus*. We could demonstrate the presence of the nanocapsules in macrophages, but, importantly, the nanocapsules did not affect cell viability and did not activate proinflammatory responses at doses up to 20 µg/mL.

Conclusion: Our bactericidal silver-containing titanium dioxide nanocapsules fulfill important prerequisites for biomedical use and represent a promising material for the coating of artificial implants.

Keywords: silver nanoparticles, titanium dioxide nanocapsules, antimicrobial effect, multidrug-resistant *S. aureus*, immune cell uptake

Introduction

Total hip or knee arthroplasty are among the most successful and widely performed orthopedic surgical procedures worldwide,[1] and can relieve pain, restore function and significantly improve quality of life. In the US, over 900′000 hip or knee replacements are performed annually and this number continues to grow.[2] However, infections after such implantations are frequent,[3] and currently range in developed countries from 0.5% to 2%.[4] Bacterial biofilms on the biomaterial's surface play an important role in the pathogenesis of prosthetic infections and are extremely difficult to treat by antibiotherapy,[5] often requiring surgical removal and replacement of the prosthesis. Infection with a multiresistant strain of *Staphylococcus aureus* (MRSA), which is a leading cause of hospital-acquired infection, is particularly feared.[6] While vancomycin is then often the last treatment option, resistance to this antibiotic is increasing.[7] It is thus essential to develop novel strategies to prevent MRSA superinfection of endoprostheses.

A promising option to prevent prosthetic infections is the development of antimicrobial implant coatings based on silver and its compounds, historically known for

Correspondence: Katharina M Fromm
University of Fribourg, PER 10 bu. 114, chemin du Musée 9, Fribourg 1700, Switzerland
Tel +41 26 300 8732
Email katharina.fromm@unifr.ch

submit your manuscript | www.dovepress.com
DovePress
http://doi.org/10.2147/IJN.S231949

their broad spectrum antimicrobial activity against bacteria,[8] fungi[9] and viruses.[10] Silver ions act in a multi-directional manner, interacting with the bacterial cell membrane, electron transport processes and DNA, which may prevent the resistance acquisition frequently observed with antibiotics.[11] Although higher silver tolerance can sometimes be observed in MRSA, bacteria carrying these genes are rare and still susceptible to silver treatment.[12,13] Recent silver-based compounds with good biocompatibility and excellent antimicrobial activity[14–18] rapidly lose their antibacterial efficacy upon diffusion, however, and this silver burst release may lead to adverse effects towards mammalian cells.[19] To regulate the release and maintain the silver ion concentration within a therapeutic range, silver nanoparticles (AgNPs) have been investigated. Their silver ion release depends on intrinsic (eg, AgNPs size/surface area, type and concentration of stabilizer) as well as external (eg, solvent, media, pH, etc.) parameters.[20,21] AgNPs in wound dressings were reported to be more active against pathogens than silver nitrate or silver sulphadiazine,[22] and showed good potential in orthodontic therapy due to their antimicrobial activity against *S. mutans* and *S. sobrinus*.[23] AgNPs have also been encapsulated in different inorganic metal oxide shells such as CeO_2,[24] CeO_2@TiO_2[25] or SiO_2,[26] resulting in longer-lasting activity.[27]

As many joint implants are made from FDA-approved titanium alloys, we have developed AgNP-containing titanium dioxide nanocapsules (Ag-TiO_2 NC) in order to reduce the direct contact of host cells with silver NPs while preserving their antimicrobial properties. Indeed, hollow titanium dioxide structures act as reservoir for cargo molecules and control their release as drug delivery system.[28]

Titanium oxide nanoparticles, eg, in sunscreens, have however raised concerns about their immunotoxicity compared to biologically inert bulk TiO_2.[29] Different studies showed the potential toxicity of TiO_2 nanoparticles, including inflammation,[30] induction of reactive oxygen species[31] and cytotoxicity in macrophages.[32] Assessing the impact of titanium dioxide nanocapsules on the immune system as a prerequisite for biomedical applications is thus essential.

The purpose of this work was therefore to study the influence of the silver content and the crystallinity of titanium dioxide in Ag-TiO_2 NC on their antimicrobial properties as well as on their biocompatibility. Our research focused on i) the reliable synthesis and characterization of Ag-TiO_2 NC with different silver contents, ii) the investigation of their antimicrobial properties, and iii) the study of their impact on cells of the immune system.

Materials and Methods

Synthesis of TiO_2 NC and Ag-TiO_2 NC

Polystyrene Template Synthesis

The anionic polystyrene spheres (PS) were synthetized following a microemulsion method from Kartsonakis et al,[33] using bi-distilled polystyrene. Sodium dodecyl sulfate (0.09 g, 0.3 mmol) and potassium persulfate (0.30 g, 1.1 mmol) were mixed in water (250 mL) for 30 mins before adding styrene (3.70 g, 35.5 mmol). The reaction mixture was kept at 80°C for 42 hrs under inert atmosphere (N_2). The final suspension was centrifuged, followed by three washing steps with water (washing/centrifuging cycles). The PS were resuspended in water for storage.

TiO_2 NC Synthesis

The formation of TiO_2 NC is based on the work of Imhof.[34] To a suspension of polystyrene spheres (500 mg) in ethanol (73 mL), polyvinylpyrrolidone (PVP, 0.672 g, molecular average 360.000) and a solution of NaCl (1.675 mL, 5 mM in water) were added under stirring (900 rpm). Titanium isopropoxide (0.756 mL) was freshly introduced into ethanol (10 mL) and quickly added to the suspension. This mixture was kept 1 min under stirring (500 rpm) and aged for 14 mins. Finally, the suspension was centrifuged and washed three times with ethanol. The solid was resuspended in the smallest amount of ethanol for drying at room temperature in a Petri dish. The polystyrene core was dissolved from the PS@TiO_2 core shell particles by dissolution into chloroform using a Soxhlet apparatus for 4 to 5 hrs, yielding amorphous titanium dioxide nanocapsules (AM). Calcination at 500°C for 2 h under air lead to anatase nanocapsules (ANA).

2 wt. % Ag-TiO_2 and 8 wt. % Ag-TiO_2 NC Synthesis

Silver nanoparticles were formed on the surface of PS before the TiO_2 coating: To a suspension of PS (500 mg) in water, silver nitrate (0.01 M, V_1 = 9.25 mL; V_2 = 13.88 mL) and polyvinylpyrrolidone ($AgNO_3$:PVP (molecular average 40.000) = 1:5, m_1 = 50 mg; m_2 = 75 mg) were introduced and kept under stirring for 30 mins. A solution of sodium borohydride (0.01 M, V_1 = 9.25 mL; V_2 = 13.88 mL) was added rapidly for silver reduction. After 3 mins, the suspension was centrifuged and washed with water. These Ag-PS particles are then used for TiO_2 coating as above for the formation of 2 wt. % Ag-TiO_2 NC (2AM and 2ANA) and 8 wt. % Ag-TiO_2 NC (8AM and 8ANA).

Characterization

The powder X-ray diffractograms on samples in 0.5 mm capillaries were recorded in transmission mode with a Stoe STADIP equipped with copper monochromator source and Mythen detector. For the Scanning Electron Microscopy, the samples were deposited on a carbon tape. The analysis was performed with a TESCAN Mira 3 LM field emission. The TEM image was recorded with a Philips CM100 Biotwin. The silver content was determined from ICP-OES measurements using a Perkin Elmer Optima 7000 DV. The zeta-potential was measured in a NanoBrook ZetaPALS Potential Analyzer. For this, the samples were dispersed in ultra-pure water using an ultrasonic bath with a concentration of 1 mg/mL and then further diluted to reach a concentration of 10 µg/mL.

Silver Release Experiments

Silver release was measured in triplicates in a semi-dynamic mode with the two media used for the biocompatibility assays of fibroblasts L929 (RPMI medium) and J774A.1 macrophages (DMEM medium).

In a 96-well plate, 5 mg of particles were introduced into the well and covered by 1.2 mL of medium (RPMI or DMEM). The plate was placed and kept in an oven at 37°C. 0.5 mL aliquots were taken for each time point and replaced by 0.5 mL fresh medium.

To each aliquot, 5 mL of water was added and the solution was filtrated using disposable syringe filters. Afterward, the silver content was determined with ICP-OES.

Bacterial Culture Experiments

Antimicrobial tests were always performed in three independent experiments, with *Escherichia coli* 25922 (*E. c.*), *Staphylococcus aureus* 113 wild-type (*S. a.* 113) and multi-resistant *Staphylococcus aureus* mecA R2954 (*S. a.* mecA).

An overnight culture of *E. c.* in Müller Hinton broth (MH, Sigma Aldrich) was diluted to 10^7 cfu/mL by comparison with the McFarland turbidity standard (DEN-1, Biosan). Glass tubes containing 1.5 mL of MH broth supplemented with 0.25, 0.5 or 1 mg/mL of the nanocapsules and 1×10^6 cfu/mL *E. c.* were incubated with shaking at 230 rpm at 37°C for 24 hrs. Hundred microliter samples were taken immediately after addition of the nanocapsules (0 h) and after 2, 4, 6, 8 and 24 h after vortexing the tubes. Appropriate dilutions were spread on MH agar in duplicate for colony count.

Overnight cultures in MH broth of *S. a.* 113 and *S. a.* mecA were grown from 6 to 8 hrs starting cultures in tryptic soy broth (soybean casein digest medium, Bacto™, BD). For the starting and overnight culture of *S. a.* mecA, 0.1 mg/mL ampicillin (Sigma Aldrich) were added. The bacterial concentrations of overnight cultures were estimated by measuring the optical density (Ultrospec 10, Biochrom) and dilution to OD 0.1 (*S. a.* 3.3×10^7 cfu/mL, *S. a.* mecA 5.4×10^7 cfu/mL).

A 48-well plate containing 0.5 mL of MH broth supplemented with 0.25, 0.5 or 1 mg/mL of the nanocapsules and 1×10^6 cfu/mL *S. a.* 113 or *S. a.* mecA was incubated with shaking at 150 rpm at 37°C for 24 hrs. Fifty microliter samples for colony count were taken immediately after addition of the nanocapsules (0 h) and after 2, 6 and 24 hrs after gently mixing the suspensions with the pipette. Appropriate dilutions were plated on MH agar in duplicate for colony count. A bactericidal effect is defined as complete prevention of colony growth on the agar plate.

Cytotoxicity and Activation Assay

J774A.1 macrophages (ATCC, TIB-67) were cultured in high glucose (4.5 g/L) DMEM (Biowest) supplemented with 10% FBS (MP Biomedicals), 2 mmol L-glutamine (Corning, Fisher Scientific), 1x sodium pyruvate (Gibco, Life Technologies) and Ciprofloxacin (Bayer).

Primary bone marrow-derived macrophages (BMDMs) and dendritic cells (BMDCs) were differentiated from bone marrow cells isolated from femur and tibia of C57BL/6JRj mice. BMDCs were generated as previously described[35] with the only difference of additionally splitting the cells (1:2 ratio) at day three of the culture. BMDMs were generated by culturing the bone marrow cells at a density of 80′000 cells/cm^2 in RPMI 1640 (Gibco) supplemented with 10% FCS (Pan Biotech), 1% penicillin/streptomycin (Gibco), 2 mmol L-glutamine (Gibco), 0.5% sodium pyruvate (Gibco) and 0.1% beta-mercaptoethanol (Gibco) containing 10 ng/mL macrophage colony-stimulating factor (M-CSF) (Miltenyi) for 6 days. Every 2 days half the medium was replaced with new medium containing fresh M-CSF.

For stimulations, cells were seeded at a density of 0.5–1×10^5 cells/well in flat-bottom 96-well plates. The stimulant lipopolysaccharide (Invivogen) was used at a working concentration of 100 ng/mL. The mouse ELISA IL-6 Kit was purchased from Biolegend and the manufacturer's protocol was followed.

For flow cytometry analysis, cells were stained with Pacific Blue or Brilliant Violet 605 anti-mouse CD80 antibody (Biolegend) and with 5 μg/mL propidium iodide (Sigma) or with Zombie Violet™ Fixable Viability Kit (Biolegend) according to manufacturer's protocol. Acquisition was carried out with the flow cytometers MACSquant (Miltenyi) and Novocyte (Acea Biosciences). Analysis was performed using the software FlowJo V10.

Mice

Female C57BL/6JRj (Charles Rivers) were housed under specific pathogen-free conditions and used at 7–14 weeks of age. Animal experimentation was conducted according to Swiss regulations.

Nanoparticle Uptake

For flow cytometry uptake assays, J774A.1 macrophages were exposed for 2 h to the FITC-labeled nanocapsules at a concentration of 10 μg/mL. After three washing steps with PBS, cells were detached and stained according to the manufacturer's protocol with Zombie violet (Biolegend) to exclude dead cells. The nanocapsules were labeled with fluorescein isothiocyanate attached to the TiO_2 surface *via* the hydroxyl group using 4-aminophenyldiazonium linker following the protocol of Scheffold et al.[36] For confocal microscopy, cells were cultured in an IBIDI 8-well microscope slide (Vitaris, 80826–5) for 2 h before adding 10 μg/mL nanocapsules. Cells were incubated overnight and then stained for 2 h with LysoTrackerTM (Blue DND-22, life technologies) at a final concentration of 75 nM. Cells were visualized using a LSM microscope (Zeiss 710 Meta).

For TEM, SEM-EDS analyses, J774A.1 macrophages were cultured in a 6-well plate at a concentration of 10^6 cells/mL (2 mL per well). After washing with PBS, nanoparticles were added at final concentrations of 10 μg/mL and incubated overnight. The next day, after removal of the cell culture media, the cells were submerged with fixative which was prepared as follows: 2.5% glutaraldehyde (Agar Scientific, Stansted, Essex, UK) in 0.15 M HEPES (Fluka, Buchs, Switzerland) with an osmolarity of 670 mOsm and adjusted to a pH of 7.35. Cells were stored in fixation solution at 4°C in the dark for 48 h. The following steps, performed at the University of Bern, include cells washing three times for 5 min with 0.15 M HEPES before adding 0.1 M Na-cacodylate buffer containing 1% OsO_4 (SPI Supplies, West Chester, USA) for 1 h at 4°C for the postfixation. For dehydration, cells were put in successive ethanol baths (70%, 80% and 96% in water) for 15 min at room temperature. Then, cells were incubated three times in 100% ethanol and two times in acetone for 10 min. Acetone/Epon (1:1) solution was added to cells overnight at room temperature before embedding them in Epon for 5 days at 60°C until solidification. First, semithin sections (1μm) were stained with a solution of 0.5% toluidine blue O (Merck, Darmstadt, Germany) for light microscopy and then ultrathin sections (ca. 50 nm) for electron microscopy. Fifty Newton meter sections were cut using a UC6 Leica ultramicrotome. Sections were mounted on single slot copper grids and stained with uranyl acetate and lead citrate with an ultrastrainer (Leica Microsystem). Sections were then examined with a transmission electron microscope (Philips CM100 Biotwin) equipped with a digital camera (Morada) and with a scanning electron microscope (FEI XL30 Sirion FEG) equipped with an Energy Dispersive Spectroscopy system.

Results

Synthesis and Characterization of Ag-TiO_2 and TiO_2 Nanocapsules (Ag-TiO_2 NC and TiO_2 NC)

Nanocapsules of titanium dioxide were obtained from a sacrificial template method inspired by Imhof.[34] After coating polystyrene (PS) spheres of 190 nm diameter with TiO_2 in presence of polyvinylpyrrolidone (PVP), solvent extraction dissolved the PS core and lead to amorphous TiO_2 NC (AM). Upon calcination, crystallization of TiO_2 to anatase (ANA) occurred. Ag-TiO_2 NC were prepared following the same pathway except that the PS spheres were partially covered with AgNPs prior to the TiO_2 coating (Figure 1). These samples were also calcined to crystallize the TiO_2 to yield the anatase form for the Ag-TiO_2 NC. For antimicrobial and biocompatibility tests, two different silver loadings, 2.0 and 8.0 wt. %, were prepared by varying the initial concentration of silver, for both amorphous and anatase TiO_2 shells, and are abbreviated as 2AM, 2ANA, and 8AM, 8ANA, respectively.

The resulting materials were investigated by scanning and transmission electron microscopy (SEM and TEM) (Figure 2). For all samples, SEM imaging demonstrated the spherical shape and uniform size of 200 ± 10 nm with a wall thickness of 20–30 nm. During the crystallization at 500°C, the TiO_2 shell shrank for all anatase samples (Figure 2A, 2, 4, 6), and holes were formed in the TiO_2 shells corresponding to intergranular porosity. On the TEM images (inserts Figure 2A), the cavity inside the nanocapsules is clearly distinguishable. While neither

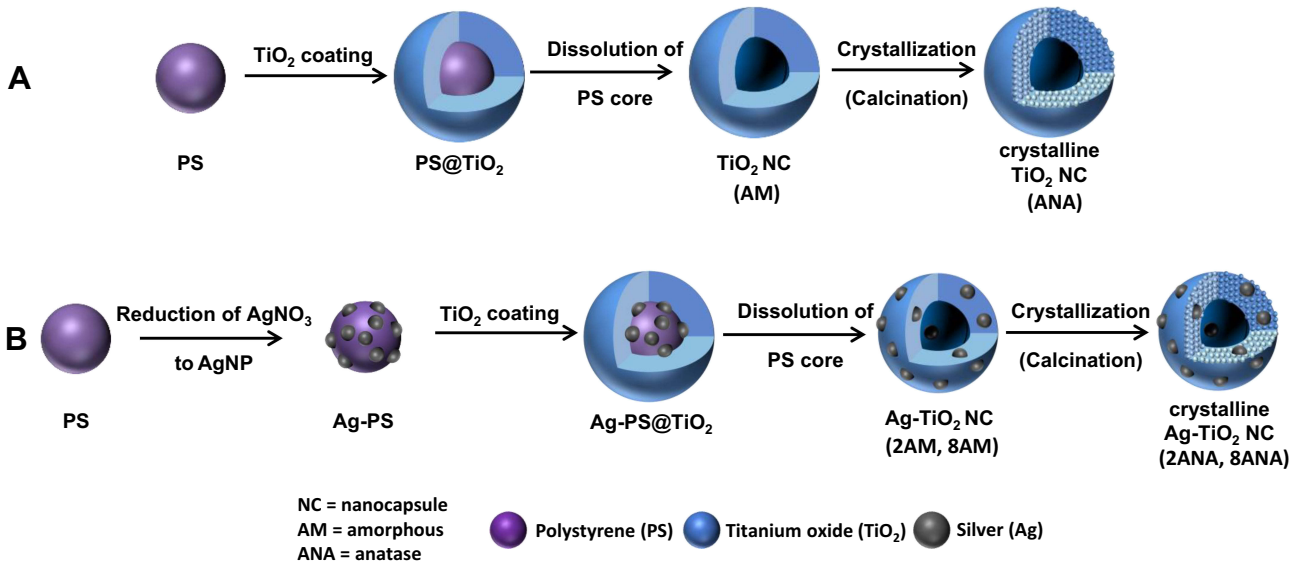

Figure 1 Synthetic pathway of (**A**) TiO_2 NC and (**B**) Ag-TiO_2 NC at 2 wt. % (2AM, 2ANA) and 8 wt. % (8AM and 8ANA).

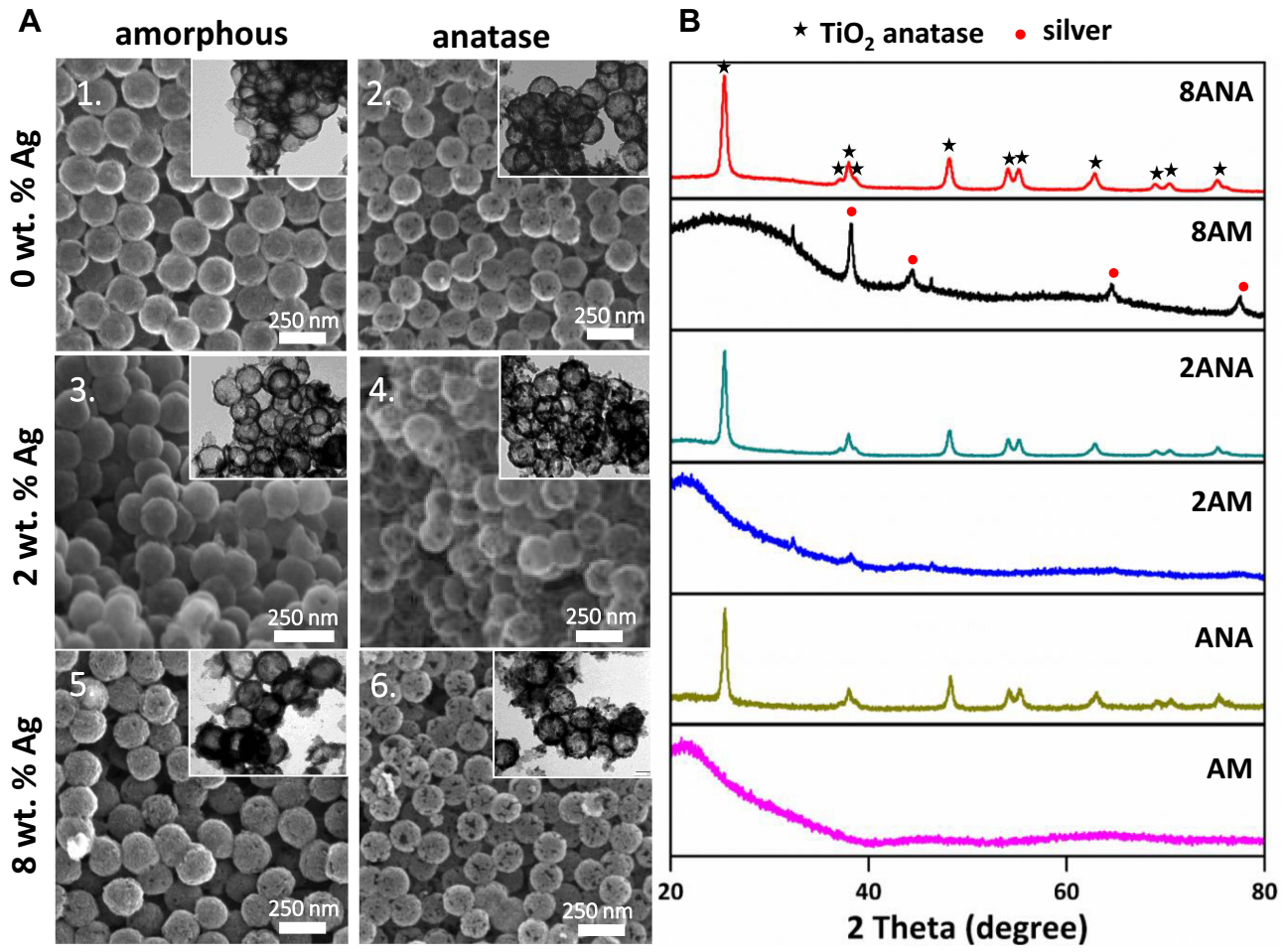

Figure 2 (**A**) SEM and TEM (inserts) images of amorphous and anatase TiO_2 NC containing 0, 2 and 8 wt. % Ag. (**B**) X-ray diffractograms of TiO_2 NC amorphous and anatase (AM, ANA), and Ag-TiO_2 NC containing 2 wt. % Ag (2AM, 2ANA), or 8 wt. % Ag (8AM, 8ANA).

SEM nor TEM could detect the AgNPs due to their small size and the low quantity, the presence of silver in the capsules was confirmed by energy-dispersive X-ray spectroscopy (EDS) analysis (Figure S1).

The transformation of amorphous TiO_2 to the crystalline anatase by thermal treatment at 500°C was detected by powder x-ray diffraction (PXRD, Figure 2B) and is in agreement with literature phase transitions[37] before forming the rutile phase of TiO_2 at around 600°C.[38]

The PXRD measurements also confirmed the presence of metallic silver for the 2AM and 8AM samples. Using the Scherrer equation, the crystallite size of the AgNPs was determined to ca. 7 and 17 nm, respectively. After calcination yielding 2ANA and 8ANA, the main Ag diffraction peak of silver at around 38.1° of 2θ overlapped with the signals of anatase-TiO_2, while the weaker signals were covered by noise. Therefore, the amount of silver in these samples was quantified with ICP-OES measurements after nitric acid treatment (Table 1).

The ζ-potential of the nanocapsules depended on the treatment to which the TiO_2 NC were subjected. All as-synthesized amorphous samples showed a negative ζ-potential, while after calcination and TiO_2 crystallization to anatase, the surface became positively charged (Table 1). The silver loading did not have an influence on this trend. The ζ-potential of particles depends on eg, the chemical composition of the particle's surface and the environmental pH.[39] For pure TiO_2, the charge is attributed to $TiOH_2^+$ or TiO^- species.[40] Upon thermal treatment, its ζ-potential and the isoelectric point are shifted to higher values and the degree of hydroxylation is lowered,[39] due to new bridging Ti-O-Ti bonds.[41] This phenomenon could explain the formation of holes in the TiO_2 shell during the formation of anatase crystallites and the surface area drop from 200 to 50 m^2/g between AM and ANA.

Table 1 Sample Designation and Characterization Data

	Name	TiO_2 phase[a]	Ag content (%)[b]	ζ-potential[c]
TiO_2 NC	AM	amorphous	0	- 21.1 ± 0.7
	ANA	anatase	0	+ 12.7 ± 0.4
Ag-TiO_2 NC	2AM	amorphous	2.0 ± 0.1	- 24.3 ± 0.5
	2ANA	anatase	2.0 ± 0.1	+ 10.2 ± 0.7
	8AM	amorphous	8.0 ± 0.1	- 28.9 ± 0.4
	8ANA	anatase	8.0 ± 0.1	+ 8.7 ± 0.8

Notes: [a]Determination by powder X-ray diffraction; [b]Determination by ICP-OES, [c]Determination by zeta potential analyzer. The table shows the mean and standard deviation.

Silver Release from the Ag-TiO_2 Nanocapsules

The release of silver ions from the nanocapsules over time was measured during incubation in two different cell culture media, RPMI and DMEM. The cumulative silver ion release, quantified by ICP-OES, is shown in Figure 3.

The Ag^+ release from anatase Ag-TiO_2 NC (2ANA and 8ANA) was higher than from their amorphous homologues. For samples containing 8 wt. % Ag, the quantity of Ag^+ released from anatase Ag-TiO_2 NC was 2–3 times the release from the amorphous nanocapsules. Moreover, the Ag^+ release rate slowed down after 9–15 days for the anatase capsules, whereas this occurred after 1–2 days for the amorphous capsules. For the samples containing 2 wt. % Ag, a similar trend was observed to a lesser extent. Although the release was higher in DMEM medium than in RPMI, the release trends were similar in both media. Thus, the crystallinity of the TiO_2 clearly modulates the release of the silver ions.

Uptake of TiO_2 NC and $AgTiO_2$ NC by Macrophages

Macrophages, innate immune cells and part of the first line defense against pathogens, are potent phagocytic cells that can take up and digest particulate material and activate other immune cells.[42] To determine whether the nanocapsules were taken up by macrophages, 8AM and 8ANA were dye-functionalized according to Scheffold et al.[36] J774A.1 macrophages were incubated with these FITC-labeled nanocapsules and uptake was assessed by flow cytometry. As shown in Figure 4A, the fluorescence intensity was clearly higher in cells incubated with the nanocapsules than in untreated control cells. The macrophages were also incubated with nanocapsules at 4°C, as low temperatures inhibit the active uptake of nanocapsules into cells.[26,43] The significantly lower fluorescence intensity at this temperature suggested that the uptake of Ag-TiO_2 NC into macrophages was

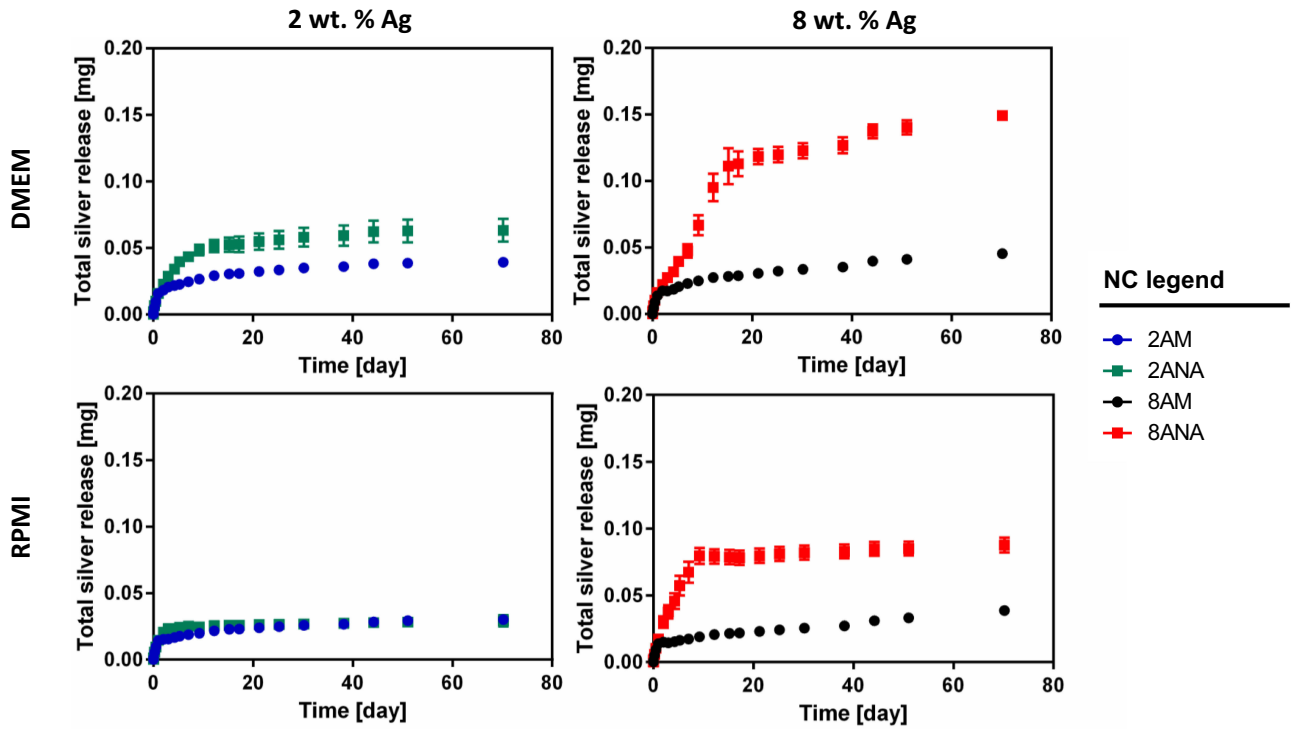

Figure 3 Total silver ion release determined by ICP-OES of amorphous and anatase Ag-TiO_2 NC containing 2 wt. % and 8 wt. % Ag in DMEM and RPMI media. The graphs show the mean and standard deviation of three independent experiments.

an active process. The fluorescence signal at 4°C remained nevertheless higher than in the untreated control, indicating that a small amount of nanocapsules may passively attach to the cell surface. Importantly, the uptake of nanocapsules did not affect the viability of the macrophages (Figure 4B).

To investigate the subcellular localization of nanocapsules, macrophages were incubated with FITC-labeled 8ANA[36] and analyzed by confocal microscopy. Particles taken up by phagocytic cells such as macrophages are normally found in the lysosomes, and indeed, Figure 4C clearly shows the co-localization of the FITC-labeled 8ANA (green) with the lysosomes (blue), demonstrating an accumulation of the nanocapsules in this intracellular compartment.

Further confirmation for the cellular particle uptake was obtained by transmission and scanning electron microscopy (TEM and SEM) using the non-fluorescent nanocapsules. Figure 5A and B shows TEM micrographs of macrophages loaded with dense particle clusters surrounded by a membrane (8AM and 8ANA, respectively), confirming an active uptake. Such clusters are lacking in the negative control (not shown).

Elemental mapping for Ti on thin sample slices demonstrated by EDS that the electron dense clusters in the TEM micrographs were indeed the nanocapsules (Figure 5 for 8ANA, Figures S3, S5 and S7 for the other nanocapsules). It further confirms the hollow nanocapsule topology, as no titanium was found inside the particles. The EDS map for Ag clearly showed a higher silver content for the lysosomes containing the Ag-TiO_2 NC than cell areas, which did not contain NCs (Figures S2, S4, S6 and S8). For example, for 2ANA, a spot analysis on the nanocapsules gave 14.8 ± 0.5 wt. % Ti and ca. 0.5 ± 0.4 wt. % Ag, whereas on a spot where no nanocapsules were seen, Ti and Ag signals were below noise levels.

Impact of TiO_2 NC and Ag-TiO_2 NC on Immune Cell Viability and on Immune Cell Function

To determine the toxicity of the nanocapsules, macrophages were incubated with increasing concentrations of amorphous and anatase TiO_2 NC and Ag-TiO_2 NC. There was no significant change in cell survival up to 20 µg/mL (Figure 6A and B). At 40 µg/mL, only 8ANA significantly affected cell viability. Furthermore, sheep red blood cells were used to determine the hemolytic activity of the nanocapsules. Up to 50 µg/mL, no lysis of red blood cells was observed (Figure S9). Additionally, the cell viability of

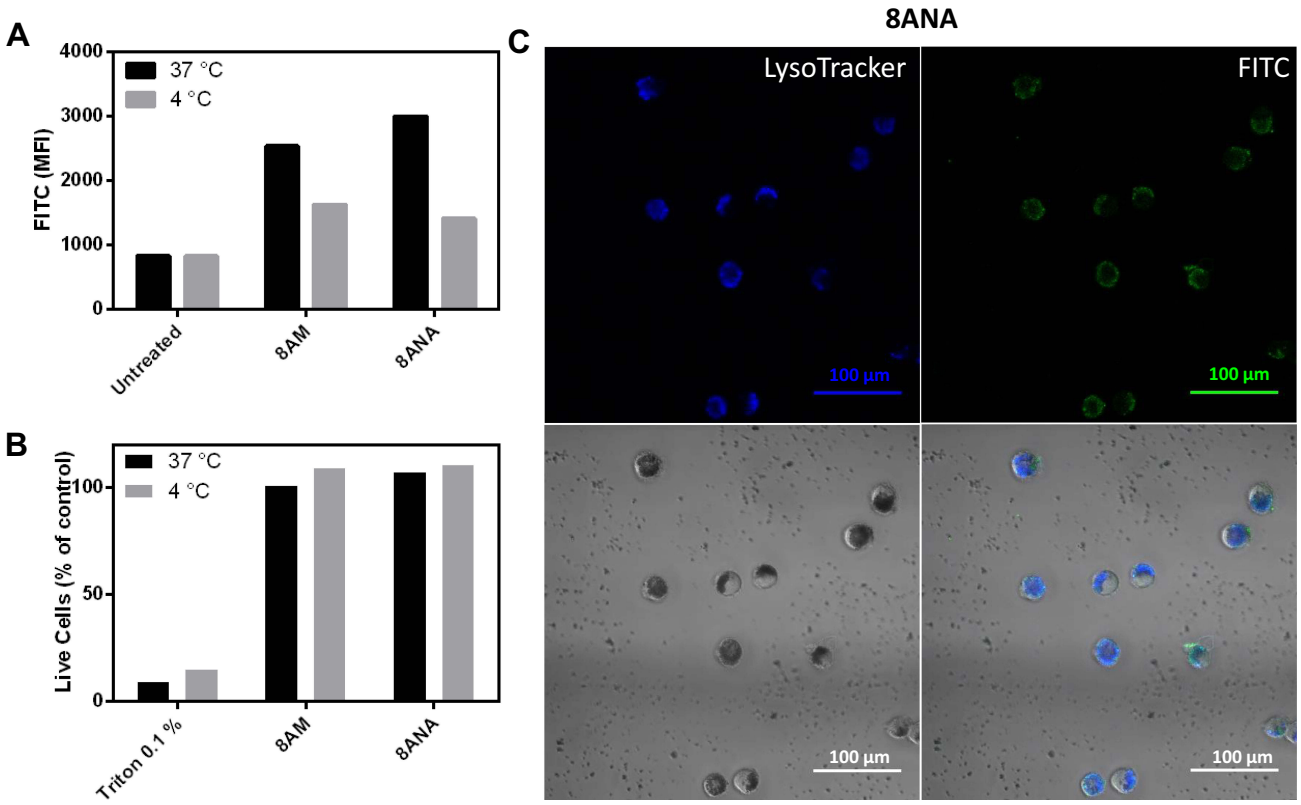

Figure 4 Ag-TiO_2 NC are taken up into the lysosomes of macrophages. J774A.1 macrophages were incubated overnight at 37°C or 4°C with 10 µg/mL FITC-labeled 8 wt. % anatase or amorphous Ag-TiO_2 NC (8ANA/8AM). (**A, B**) Mean fluorescence intensity (MFI) in live macrophages (**A**) and macrophage viability (**B**) was measured by flow cytometry. Triton X-100 (0.1%) was used as negative control. The graphs show the mean of two independent experiments. (**C**) LSM images of macrophages were taken after overnight incubation with 10 µg/mL FITC-labeled 8ANA (green). The lysosomes of the cells were stained with LysoTracker™ (blue).

fibroblasts (murine L929 cell line) was not affected up to 10 µg/mL (Figure S10).

To test if the macrophages become activated through nanocapsule uptake, the production of the pro-inflammatory cytokine interleukin 6 (IL-6)[42] was measured after 24 h incubation of macrophages with Ag-TiO_2 NC or TiO_2 NC. As positive control, macrophages were incubated with lipopolysaccharide (LPS), a bacterial cell wall component known to be a potent activator of macrophages.[44] None of the tested Ag-TiO_2 NC and TiO_2 NC concentrations led to IL-6 secretion, while the positive control with LPS produced high amounts of IL-6 (Figure 6C and D). Furthermore, the up-regulation of the co-stimulatory molecule CD80, a marker for immune activation, was determined by flow cytometry on the surface of macrophages. As shown in Figure 6E and F, CD80 was not upregulated in macrophages in presence of the nanocapsules. Importantly, the viability and activation assays were performed on both a murine macrophage cell line and primary mouse bone marrow-derived macrophages (BMDMs) and dendritic cells (BMDCs). No difference in viability nor activation was observed between the cell line and the primary cells (Figures 6 and S11). Hence, Ag-TiO_2 NC and TiO_2 NC do not cause immunological activation of macrophages at concentrations up to 20 µg/mL.

Antimicrobial Properties of Silver-Containing TiO_2 Nanocapsules

The antimicrobial efficacy of the Ag-TiO_2 NC was first studied on *Escherichia coli* (*E. coli*), which can cause periprosthetic infections.[14] Liquid bacterial cultures were supplemented with three different concentrations of TiO_2 NC or Ag-TiO_2 NC and bacterial growth was determined at the indicated time points (Figure 7). The antimicrobial effect was clearly dependent on the applied dose, on the silver content and on the crystallinity of the TiO_2 shell. Particles without silver cargo did not show any bactericidal effect (Figure 7A and D), while anatase Ag-TiO_2 NC had a stronger bactericidal effect compared to amorphous Ag-TiO_2 NC (Figure 7B, C, E and F). Amorphous Ag-TiO_2 NC were bactericidal only at the highest concentration of 1 mg/mL, whereas the anatase Ag-TiO_2 NC already showed bactericidal

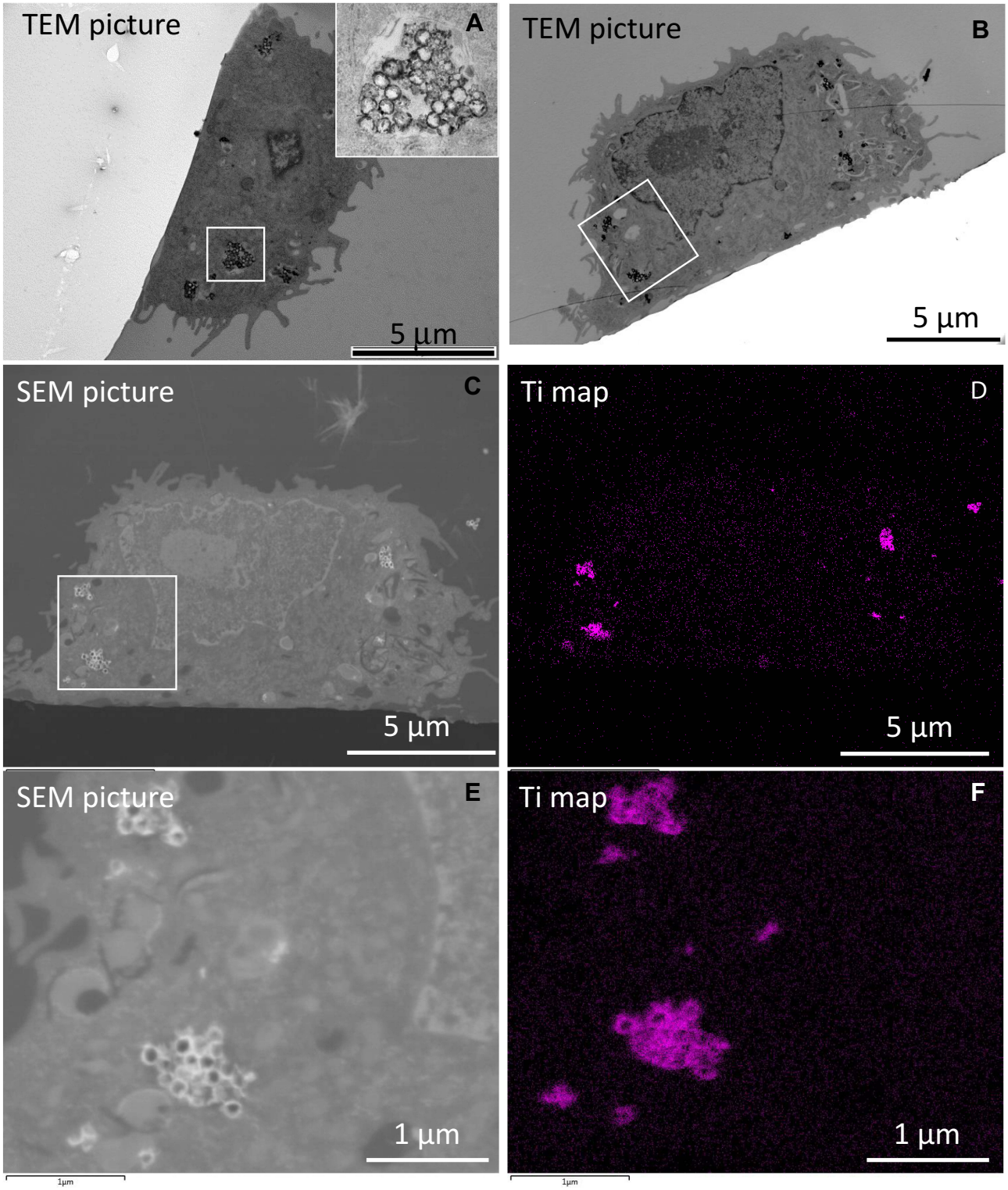

Figure 5 (**A**) TEM images of the macrophages after incubation with 8AM. (**B**–**F**) TEM (**B**), SEM images (**C, E**) and the corresponding titanium map (**D, F**) of the macrophages after incubation with 8ANA. J774 macrophages were incubated at 37°C overnight with nanocapsules at a concentration of 10 µg/mL (8ANA).

activity at lower concentrations of 0.5 mg/mL (2ANA) and 0.25 mg/mL (8ANA). No significant differences between the antimicrobial efficacy of 2AM and 8AM were observed, while 8ANA was clearly more effective than 2ANA; a trend in line with the silver ion release profiles.

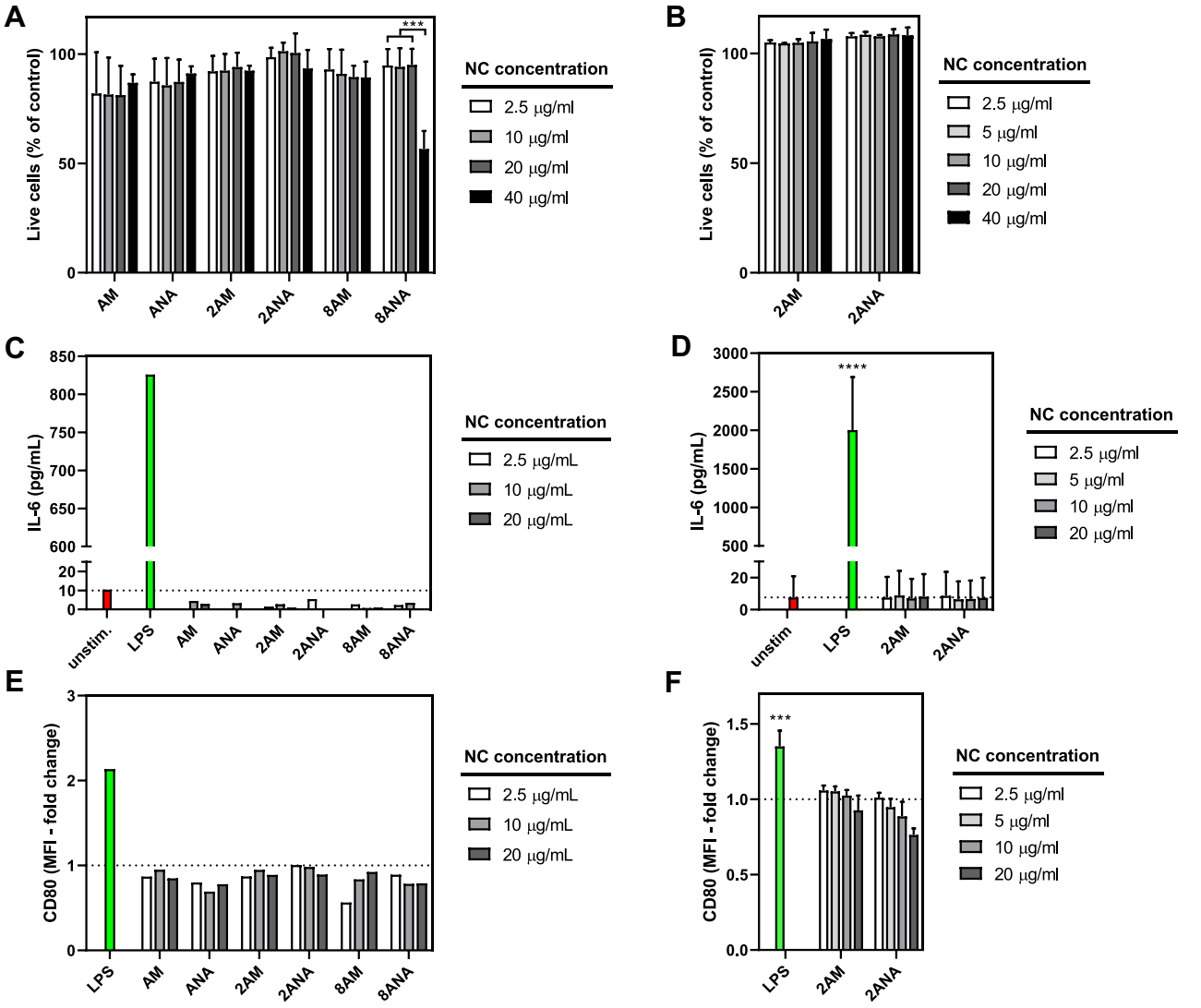

Figure 6 Impact of TiO_2 NC and Ag-TiO_2 NC on viability and activation of macrophages. The J774A.1 macrophage cell line (**A, C, E**) or primary mouse bone marrow-derived macrophages (BMDMs) (**B, D, F**) were incubated at 37 °C for 24 h with different concentrations of TiO_2 NC and Ag-TiO_2 NC. (**A, B**) Viability was assessed with propidium iodide or Zombie violet staining by flow cytometry. Live cell percentages refer to control cells incubated without nanocapsules. The graphs show the mean and standard deviation of three independent experiments. The only significant statistical difference is found between the lower concentrations (2.5, 10 and 20 µg/mL) and the highest concentration (40 µg/mL) of 8ANA as determined by two-way ANOVA ($p^{***}<0.001$). (**C, D**) The production of the pro-inflammatory cytokine IL-6 was determined in the cell culture supernatants by ELISA. Lipopolysaccharide (LPS) was included as positive control. The IL-6 production by LPS is significantly higher compared to all Ag-TiO_2 NC groups as determined by one-way ANOVA ($p^{****}<0.0001$) (**E, F**) The surface expression of the costimulatory molecule CD80 was assessed by flow cytometry. The mean fluorescence intensity (MFI) of CD80 in live cells is expressed relative to the unstimulated control. The fold-change of CD80 in BMDMs induced by LPS is significantly higher compared to 2ANA or 2AM as determined by one-way ANOVA ($p^{***}<0.001$) The graphs show the mean of two independent experiments (**C, E**) or the mean and standard deviation of three independent experiments (**D, F**).

Considering their clinical importance in prosthetic infections, the antimicrobial activity of Ag-TiO_2 NC was determined on wild-type and multidrug-resistant *S. aureus* mecA (Figure 8). The highest dose of 1 mg/mL of 8ANA was bactericidal for wild-type *S. aureus*, whereas lower concentrations of 8ANA and all tested concentrations of 8AM inhibited bacterial growth at least in part (Figure 8A and C). Exposure of the multidrug-resistant *S. aureus* strain mecA R2954 to the 8AM and 8ANA resulted in the same growth behavior as seen for wild type *S. aureus*, with the highest dose of 8ANA being able to kill all bacteria (Figure 8B and D).

Discussion

We have developed and characterized Ag-containing TiO_2 nanocapsules (Ag-TiO_2 NC) with potent antimicrobial properties. For biomedical applications, reproducibility of nanoparticle synthesis is essential, as moderate differences

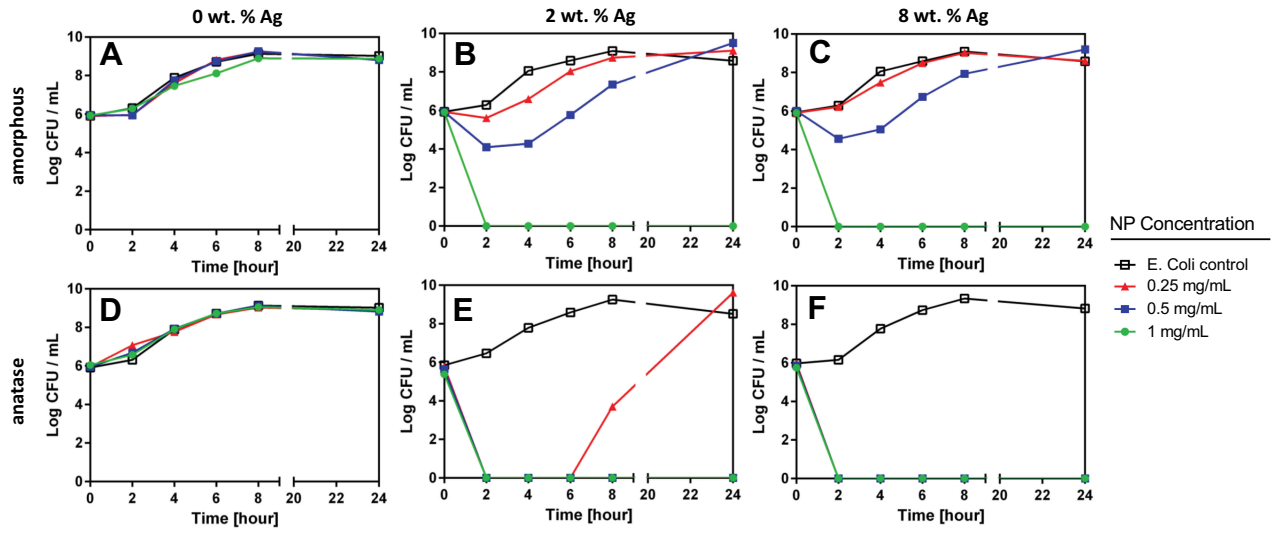

Figure 7 Antimicrobial effect of amorphous (**A-C**) and anatase (**D-F**) Ag-TiO_2 NC on the growth of *E. coli.* Bacterial cultures of *E. coli* 25922 in Müller Hinton broth were supplemented with 3 different concentrations of TiO_2 NC (**A, D**), 2 wt. % Ag-TiO_2 NC (**B, E**) and 8 wt. % Ag-TiO_2 NC (**C, F**). Samples were taken at the indicated time points to determine the bacterial growth on agar plates. The graphs are representative of three independent experiments.

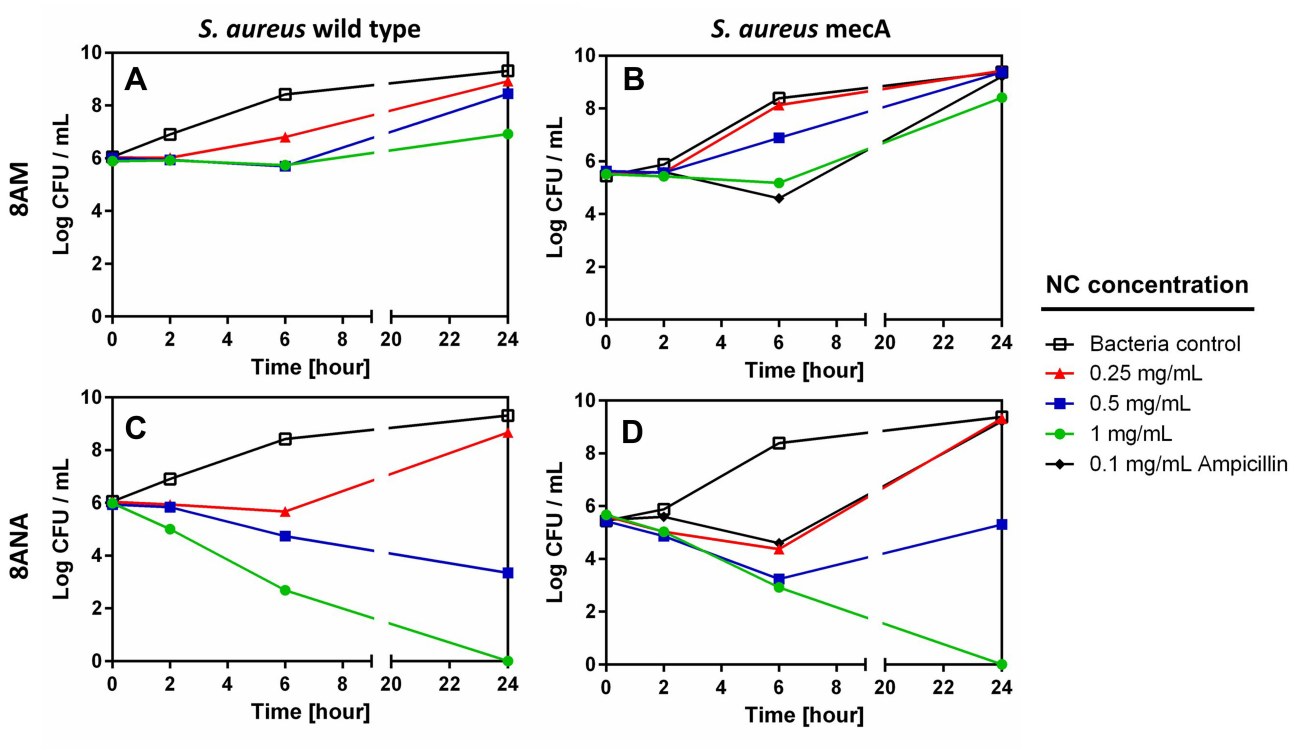

Figure 8 Antimicrobial effect of amorphous and anatase Ag-TiO_2 NC containing 8 wt. % Ag on the growth of *S. aureus*. Bacterial cultures of *S. aureus* 113 wild type (**A, C**) or multiresistant *S. aureus* mecA R2954 (**B, D**) in Müller Hinton broth were supplemented with 3 different concentrations of either 8AM (**A, B**) or 8ANA (**C, D**). At the indicated time points samples were taken to determine the bacterial growth on agar plates. The graphs are representative of three independent experiments.

in physicochemical properties can lead to changes in biocompatibility, in particular with respect to immune cells.[45] In a straightforward and highly reproducible synthesis, TiO_2 NC with tunable AgNP content and a diameter of 200 ± 10 nm were obtained at low temperature in their amorphous state.[46] Polymeric capping agents, like remaining PS and PVP, may be responsible for the decrease of the dissolution rate of AgNPs.[47] In comparison, the higher Ag^+

ion release from anatase Ag-TiO_2 NC, formed at 500°C, might be explained by intergranular pores that are formed by decomposition of residual polymers. While the surface charge measured for amorphous nanocapsules was negative, the anatase homologue unexpectedly showed a positive surface charge. Generally, the surface charge depends on the pH,[48] which was close to pH 7 as the Ag-TiO_2 formulations were dispersed in water. Interestingly, it has been shown that depending on the precursors used to generate titania, on the surfactant and on the heat treatment, the surface charge can indeed become positive even at pH 7.[39] In another publication, the surface charge was positive throughout all pH ranges,[40] and it has been shown that the presence of cations like zinc can influence the zeta potential and render it positive.[49] Thus, there is evidence that positive zeta potentials may occur at pH 7. In our case, the presence of silver ions on the surface of the nanoparticles may very well increase during the heating procedure and may therefore induce a sign change in the zeta potential.

The antimicrobial activity of the Ag-TiO_2 NC mirrored the Ag^+ release: Anatase and higher loaded Ag-TiO_2 NC showed a stronger antibacterial effect than amorphous and lower loaded nanocapsules, suggesting that the antibacterial activity of the nanocapsules was indeed due to the Ag^+ release.[47,50] Furthermore, positively charged nanoparticles[51,52] adhere better to negatively charged bacterial membranes,[53] thus also explaining the strong antimicrobial efficacy of the anatase Ag-TiO_2 NC. The continuous silver release over at least 70 days demonstrates the long-term antibacterial potential of the Ag-TiO_2 NC.[4]

Ag-TiO_2 NC efficiently killed both Gram-negative *E. coli* and Gram-positive *S. aureus*, including even an antibiotic-resistant strain of *S. aureus*. This highlights the potential use of Ag-based therapeutic strategies where antibiotics have failed.[54]

Fluorescently labelled Ag-TiO_2 NC were readily taken up by a macrophage cell line in an active process, similar to Ag@SiO_2 systems.[26] We have previously shown for other types of fluorescently labelled nanoparticles that the uptake in this macrophage cell line mirrors the uptake seen in primary murine antigen-presenting cells.[55,56] The uptake of non-fluorescent NCs by macrophages was proven by TEM, SEM and elemental mapping experiments, showing hollow particles made of TiO_2 inside the cells. Comparing EDS spectra, intracellular silver concentrations were found to be higher in the intracellular nanocapsules than in NC-free areas of the cell. Our approach unambiguously proved the presence of Ag-TiO_2 NC in the cell, whereas previous studies on nanoparticle uptake were usually limited to TEM[57] and fluorescence[58,59] without proof of the particle composition. One publication reports on parallel electron-energy loss (PEEL) spectroscopy on 20 nm iron oxide nanocapsules in macrophages[60] without, however, visualizing the capsule cavity after cellular uptake.

Despite uptake into macrophages, no proinflammatory response nor cytotoxicity in these cells were detected for our nanocapsules, except for 8ANA at the highest concentration (40 µg/mL). This is an important finding, since full TiO_2 nanoparticles from 25 to 100 nm were reported to induce inflammatory cytokine production and affect cell viability already at concentrations of 10 µg/mL.[61,62] An extensive proteomic analysis demonstrated that full TiO_2 spheres between 20 and 100 nm can cause DNA damage, oxidative stress, and apoptotic cell death in stem cells from 10 µg/mL.[62,63] In contrast to the well-characterized Ag-TiO_2 NC synthesized for this work, these and other studies of full TiO_2 particles have used commercially available, polydisperse preparations with diameters varying between 20 and 100 nm. The greater diameter of our Ag-TiO_2 NC may reduce uptake by non-phagocytic cells and thus prevent unwanted side effects. Another important consideration is that some of the AgTiO_2 NC precipitate, form agglomerates and sediment in solution. As a consequence the effective concentration for bacterial killing is overestimated as the bacteria in broth are exposed to a lower AgTiO_2 NC concentration. For a 2D cell culture, grown on the bottom of the well, it is exactly the opposite. Precipitation of the particles or of released silver ion – protein conjugates will increase the effective concentration for the cells.[64] Also important when assessing biocompatibility is the difference of two-dimensional (2D) cell cultures versus real life, in which different cell types are in a three-dimensional (3D), non-static environment. Cells in a 3D system tolerate higher silver concentrations than in a 2D system, which further supports the probability of success of such a material as coating for prosthetic joints.[65,66] In an in vivo setting rather than in cell cultures, the therapeutic window may therefore be improved.

Since many joint and hip endoprostheses are already constituted of titanium-containing alloys, Ag-TiO_2 NC could readily serve as antibacterial coating for these prosthetics. The Ag-TiO_2 NC could be covalently attached to the surface of the implant by functionalization of the Ti-OH groups from the capsules and/or the implant surface, or embedded into a surface coating. The confirmed silver release over 70 days corresponds to a time window during

which acute post-operative joint infections occur,[6] offering antibacterial protection during this critical period. It is probable that the silver ions released from the coated nanocapsules would be concentrated at the site of the implant and may thus reach the necessary antibacterial concentrations determined in this study. Indeed, it was shown that surface immobilized rather than colloidal AgNPs show greater efficacy in bacterial killing and that the therapeutic window is increased at the coating surface.[67,68] In contrast, it is probable that the phagocytic immune cells in the prosthesis environment would be exposed to lower concentrations of the particles than those tested in this study, as the NC will be immobilized on the implant surface. Further studies are needed to determine whether this is indeed the case and whether the implant coating can be both bactericidal and biocompatible in an in vivo setting.

Conclusion

In summary, amorphous and anatase Ag-TiO_2 NC were reproducibly synthesized and are biocompatible independently of their silver ion release, with dose-dependent antibacterial properties against a multiresistant strain of *S. aureus*. For the first time, moreover, nanocapsule uptake in cellular compartments of macrophages was coclusively demonstrated through an analysis of the nanocapsules' chemical composition and topology. Overall, the Ag-TiO_2 NC presented here combine a number of important properties, making them valuable candidates for antimicrobial drug delivery.

Abbreviations

MRSA, multiresistant strain of Staphylococcus aureus; AgNP, silver nanoparticles; NC, nanocapsules; ANA, anatase nanocapsules; AM, amorphous nanocapsules.

Acknowledgments

We are grateful to Priscilla S. Brunetto for her help in the correction of the article and Christoph Neururer for the SEM-EDS images. Electron microscopy sample preparation of the cells after particle uptake was performed with devices supported by the Microscopy Imaging Center (MIC) of the University of Bern. We are thankful to Prof. Patrice Nordmann for providing *S. aureus* mecA strain and to Prof. Nina Khanna for providing *S. aureus* wild type.

Author Contributions

Nelly Hérault performed the synthesis and the physico-chemical characterizations, silver release experiments, electron microscopy images and the particles labeling. Julia Wagner performed the cytotoxicity and activation assays on J774A.1 macrophages and primary mouse cells. Sarah-Luise Abram carried out the antimicrobial tests on *E. coli, S. aureus* and *S. aureus* mecA. Lenke Horvath carried out the cytotoxicity assays on L929 fibroblasts. Jérôme Widmer was responsible for cytotoxicity assays on J774A.1 macrophages, hemolysis assay, confocal microscopy and the cell fixation. Dimitri Vanhecke gave input and helped on electron microscopy and EDS map on the cells cut sections. Carole Bourquin and Katharina M. Fromm designed and supervised the study. All authors contributed to data analysis, drafting or revising the article, gave final approval of the version to be published, and agreed to be accountable for all aspects of the work.

Funding

This research was financially supported by the Swiss Competence Center in Energy Research (SCCER) for Heat and Electricity Storage, the National Competence Center in Research (NCCR) Bio-Inspired Materials (Grant Number 51NF40_141849), the Swiss National Science Foundation (grant numbers 156372 and 156871), and the Commission for Technology and Innovation (CTI). We are also grateful to the University of Fribourg, the Adolphe Merkle Foundation and the FriMat for their support.

Disclosure

The authors report no conflicts of interest in this work.

References

1. Kurtz S, Ong K, Lau E, Mowat F, Halpern M. Projections of primary and revision hip and knee arthroplasty in the United States from 2005 to 2030. *J Bone Joint Surg Am*. 2007;89(4):780–785. doi:10.2106/JBJS.F.00222
2. Maradit Kremers H, Larson DR, Crowson CS, et al. Prevalence of total hip and knee replacement in the United States. *J Bone Joint Surg Am*. 2015;97(17):1386–1397. doi:10.2106/JBJS.N.01141
3. Springer BD, Cahue S, Etkin CD, Lewallen DG, McGrory BJ. Infection burden in total hip and knee arthroplasties: an international registry-based perspective. *Arthroplast Today*. 2017;3(2):137–140. doi:10.1016/j.artd.2017.05.003
4. Lindeque B, Hartman Z, Noshchenko A, Cruse M. Infection after primary total hip arthroplasty. *Orthopedics*. 2014;37(4):257–265. doi:10.3928/01477447-20140401-08
5. Donlan RM, Costerton JW. Biofilms: survival mechanisms of clinically relevant microorganisms. *Clin Microbiol Rev*. 2002;15(2):167–193. doi:10.1128/CMR.15.2.167-193.2002

6. Zimmerli W, Trampuz A, Ochsner PE. Prosthetic-joint infections. *N Engl J Med*. 2004;351(16):1645–1654. doi:10.1056/NEJMra040181
7. Appelbaum PC. The emergence of vancomycin-intermediate and vancomycin-resistant Staphylococcus aureus. *Clin Microbiol Inf*. 2006;12(Suppl 1):16–23. doi:10.1111/j.1469-0691.2006.01344.x
8. Kim JS, Kuk E, Yu KN, et al. Antimicrobial effects of silver nanoparticles. *Nanomed*. 2007;3(1):95–101. doi:10.1016/j.nano.2006.12.001
9. Sadhasivam S, Shanmugam P, Yun K. Biosynthesis of silver nanoparticles by Streptomyces hygroscopicus and antimicrobial activity against medically important pathogenic microorganisms. *Colloids Surf B Biointerfaces*. 2010;81(1):358–362. doi:10.1016/j.colsurfb.2010.07.036
10. Lu L, Sun RW, Chen R, et al. Silver nanoparticles inhibit hepatitis B virus replication. *Antivir Ther*. 2008;13(2):253–262.
11. Eckhardt S, Brunetto PS, Gagnon J, Priebe M, Giese B, Fromm KM. Nanobio silver: its interactions with peptides and bacteria, and its uses in medicine. *Chem Rev*. 2013;113(7):4708–4754. doi:10.1021/cr300288v
12. Finely P, Peterson A, Huckfeldt R. The prevalence of phenotypic silver resistance in clinical isolates. *Wounds*. 2013;25(4):84–88.
13. Loh JV, Percival SL, Woods EJ, Williams NJ, Cochrane CA. Silver resistance in MRSA isolated from wound and nasal sources in humans and animals. *Int Wound J*. 2009;6(1):32–38. doi:10.1111/iwj.2009.6.issue-1
14. Sendi P, Banderet F, Graber P, Zimmerli W. Periprosthetic joint infection following Staphylococcus aureus bacteremia. *J Infect*. 2011;63(1):17–22. doi:10.1016/j.jinf.2011.05.005
15. Slenters TV, Hauser-Gerspach I, Daniels AU, Fromm KM. Silver coordination compounds as light-stable, nano-structured and anti-bacterial coatings for dental implant and restorative materials. *J Mater Chem*. 2008;18(44):5359–5362. doi:10.1039/b813026d
16. Gordon O, Vig Slenters T, Brunetto PS, et al. Silver coordination polymers for prevention of implant infection: thiol interaction, impact on respiratory chain enzymes, and hydroxyl radical induction. *Antimicrob Agents Chemother*. 2010;54(10):4208–4218. doi:10.1128/AAC.01830-09
17. Kuehl R, Brunetto PS, Woischnig AK, et al. Preventing Implant-Associated Infections by Silver Coating. *Antimicrob Agents Chemother*. 2016;60(4):2467–2475. doi:10.1128/AAC.02934-15
18. Brunetto PS, Slenters TV, Fromm KM. In vitro Biocompatibility of new silver(I) coordination compound coated-surfaces for dental implant applications. *Materials*. 2011;4(2):355–367. doi:10.3390/ma4020355
19. Hackenberg S, Scherzed A, Kessler M, et al. Silver nanoparticles: evaluation of DNA damage, toxicity and functional impairment in human mesenchymal stem cells. *Toxicol Lett*. 2011;201(1):27–33. doi:10.1016/j.toxlet.2010.12.001
20. Reidy B, Haase A, Luch A, Dawson KA, Lynch I. Mechanisms of silver nanoparticle release, transformation and toxicity: a critical review of current knowledge and recommendations for future studies and applications. *Materials*. 2013;6(6):2295–2350. doi:10.3390/ma6062295
21. Molleman B, Hiemstra T. Time, pH, and size dependency of silver nanoparticle dissolution: the road to equilibrium. *Environ Sci-Nano*. 2017;4(6):1314–1327. doi:10.1039/C6EN00564K
22. Dakal TC, Kumar A, Majumdar RS, Yadav V. Mechanistic basis of antimicrobial actions of silver nanoparticles. *Front Microbiol*. 2016;7:1831. doi:10.3389/fmicb.2016.01831
23. Lee SJ, Heo M, Lee D, et al. Preparation and characterization of antibacterial orthodontic resin containing silver nanoparticles. *Appl Surf Sci*. 2018;432:317–323. doi:10.1016/j.apsusc.2017.04.030
24. Gagnon J, Clift MJD, Vanhecke D, et al. Integrating silver compounds and nanoparticles into ceria nanocontainers for antimicrobial applications. *J Mater Chem B*. 2015;3(9):1760–1768. doi:10.1039/C4TB02079K
25. Gagnon J, Clift MJD, Vanhecke D, et al. Synthesis, characterization, antibacterial activity and cytotoxicity of hollow TiO_2-coated CeO_2 nanocontainers encapsulating silver nanoparticles for controlled silver release. *J Mater Chem B*. 2016;4(6):1166–1174. doi:10.1039/C5TB01917F
26. Priebe M, Widmer J, Suhartha Lowa N, et al. Antimicrobial silver-filled silica nanorattles with low immunotoxicity in dendritic cells. *Nanomed*. 2017;13(1):11–22. doi:10.1016/j.nano.2016.08.002
27. Damm C, Munstedt H. Kinetic aspects of the silver ion release from antimicrobial polyamide/silver nanocomposites. *Appl Phys a-Mater*. 2008;91(3):479–486. doi:10.1007/s00339-008-4434-1
28. Zhao L, Wang H, Huo K, et al. Antibacterial nano-structured titania coating incorporated with silver nanoparticles. *Biomaterials*. 2011;32(24):5706–5716. doi:10.1016/j.biomaterials.2011.04.040
29. Lindenschmidt RC, Driscoll KE, Perkins MA, Higgins JM, Maurer JK, Belfiore KA. The comparison of a fibrogenic and two nonfibrogenic dusts by bronchoalveolar lavage. *Toxicol Appl Pharmacol*. 1990;102(2):268–281. doi:10.1016/0041-008X(90)90026-Q
30. Shi H, Magaye R, Castranova V, Zhao J. Titanium dioxide nanoparticles: a review of current toxicological data. *Part Fibre Toxicol*. 2013;10:15. doi:10.1186/1743-8977-10-15
31. Bhattacharya K, Davoren M, Boertz J, Schins RP, Hoffmann E, Dopp E. Titanium dioxide nanoparticles induce oxidative stress and DNA-adduct formation but not DNA-breakage in human lung cells. *Part Fibre Toxicol*. 2009;6:17. doi:10.1186/1743-8977-6-17
32. Rotoli BM, Bussolati O, Costa AL, et al. Comparative effects of metal oxide nanoparticles on human airway epithelial cells and macrophages. *J Nanopart Res*. 2012;14:9. doi:10.1007/s11051-012-1069-0
33. Kartsonakis IA, Liatsi P, Danilidis I, Bouzarelou D, Kordas G. Synthesis, characterization and antibacterial action of hollow titania spheres. *J Phys Chem Solids*. 2008;69(1):214–221. doi:10.1016/j.jpcs.2007.08.071
34. Imhof A. Preparation and characterization of titania-coated polystyrene spheres and hollow titania shells. *Langmuir*. 2001;17(12):3579–3585. doi:10.1021/la001604j
35. Helft J, Bottcher J, Chakravarty P, et al. GM-CSF mouse bone marrow cultures comprise a heterogeneous population of CD11c(+) MHCII(+) macrophages and dendritic cells. *Immunity*. 2015;42(6):1197–1211. doi:10.1016/j.immuni.2015.05.018
36. Dechezelles JF, Griffete N, Dietsch H, Scheffold F. A general method to label metal oxide particles with fluorescent dyes using aryldiazonium salts. *Part Part Syst Charact*. 2013;30(7):579–583. doi:10.1002/ppsc.201300014
37. Albetran H, O'Connor BH, Low IM. Effect of calcination on band gaps for electrospun titania nanofibers heated in air–argon mixtures. *Mater Des*. 2016;92:480–485. doi:10.1016/j.matdes.2015.12.044
38. Hanaor DAH, Sorrell CC. Review of the anatase to rutile phase transformation. *J Mater Sci*. 2010;46(4):855–874. doi:10.1007/s10853-010-5113-0
39. Liao DL, Wu GS, Liao BQ. Zeta potential of shape-controlled TiO2 nanoparticles with surfactants. *Colloid Surf A*. 2009;348(1–3):270–275. doi:10.1016/j.colsurfa.2009.07.036
40. Li Y, Qin Z, Guo H, et al. Low-temperature synthesis of anatase TiO2 nanoparticles with tunable surface charges for enhancing photocatalytic activity. *PLoS One*. 2014;9(12):e114638. doi:10.1371/journal.pone.0114638
41. Lv K, Cheng B, Yu J, Liu G. Fluorine ions-mediated morphology control of anatase TiO2 with enhanced photocatalytic activity. *Phys Chem Chem Phys*. 2012;14(16):5349–5362. doi:10.1039/c2cp23461k
42. Mosser DM, Edwards JP. Exploring the full spectrum of macrophage activation. *Nat Rev Immunol*. 2008;8(12):958–969. doi:10.1038/nri2448
43. Doherty GJ, McMahon HT. Mechanisms of endocytosis. *Annu Rev Biochem*. 2009;78:857–902. doi:10.1146/annurev.biochem.78.081307.110540

44. Cohen J. The immunopathogenesis of sepsis. *Nature*. 2002;420(6917):885–891. doi:10.1038/nature01326
45. Mottas I, Milosevic A, Petri-Fink A, Rothen-Rutishauser B, Bourquin C. A rapid screening method to evaluate the impact of nanoparticles on macrophages. *Nanoscale*. 2017;9(7):2492–2504. doi:10.1039/C6NR08194K
46. Herault N, Fromm KM. Influence of the sacrificial polystyrene removal pathway on the TiO2 nanocapsule structure. *Helv Chim Acta*. 2017;100(6):e1700014. doi:10.1002/hlca.v100.6
47. Liu J, Sonshine DA, Shervani S, Hurt RH. Controlled release of biologically active silver from nanosilver surfaces. *ACS Nano*. 2010;4(11):6903–6913. doi:10.1021/nn102272n
48. Verhovšek D, Veronovski N, Lavrenčič Štangar U, Kete M, Žagar K, Čeh M. The synthesis of anatase nanoparticles and the preparation of photocatalytically active coatings based on wet chemical methods for self-cleaning applications. *Int J Photoenergy*. 2012;2012:1–10. doi:10.1155/2012/329796
49. Khalameida S, Skwarek E, Janusz W, Sydorchuk V, Leboda R, Skubiszewska-Zieba J. Electokinetic and adsorption properties of different titanium dioxides at the solid/solution interface. *Central Eur J Chem*. 2014;12(11):1194–1205. doi:10.2478/s11532-014-0568-5
50. Xiu ZM, Zhang QB, Puppala HL, Colvin VL, Alvarez PJ. Negligible particle-specific antibacterial activity of silver nanoparticles. *Nano Lett*. 2012;12(8):4271–4275. doi:10.1021/nl301934w
51. Khan SS, Mukherjee A, Chandrasekaran N. Studies on interaction of colloidal silver nanoparticles (SNPs) with five different bacterial species. *Colloids Surf B Biointerfaces*. 2011;87(1):129–138. doi:10.1016/j.colsurfb.2011.05.012
52. Ivask A, Elbadawy A, Kaweeteerawat C, et al. Toxicity mechanisms in Escherichia coli vary for silver nanoparticles and differ from ionic silver. *ACS Nano*. 2014;8(1):374–386. doi:10.1021/nn4044047
53. Klodzinska E, Szumski M, Dziubakiewicz E, et al. Effect of zeta potential value on bacterial behavior during electrophoretic separation. *Electrophoresis*. 2010;31(9):1590–1596. doi:10.1002/elps.v31:9
54. Cavassin ED, de Figueiredo LF, Otoch JP, et al. Comparison of methods to detect the in vitro activity of silver nanoparticles (AgNP) against multidrug resistant bacteria. *J Nanobiotechnology*. 2015;13:64. doi:10.1186/s12951-015-0120-6
55. Widmer J, Thauvin C, Mottas I, et al. Polymer-based nanoparticles loaded with a TLR7 ligand to target the lymph node for immunostimulation. *Int J Pharm*. 2018;535(1–2):444–451. doi:10.1016/j.ijpharm.2017.11.031
56. Thauvin C, Widmer J, Mottas I, et al. Development of resiquimod-loaded modified PLA-based nanoparticles for cancer immunotherapy: a kinetic study. *Eur J Pharm Biopharm*. 2019;139:253–261. doi:10.1016/j.ejpb.2019.04.007
57. Kolosnjaj-Tabi J, Just J, Hartman KB, et al. Anthropogenic carbon nanotubes found in the airways of parisian children. *EBioMedicine*. 2015;2(11):1697–1704. doi:10.1016/j.ebiom.2015.10.012
58. Treuel L, Jiang X, Nienhaus GU. New views on cellular uptake and trafficking of manufactured nanoparticles. *J R Soc Interface*. 2013;10(82):20120939. doi:10.1098/rsif.2012.0939
59. Halamoda Kenzaoui B, Chapuis Bernasconi C, Guney-Ayra S, Juillerat-Jeanneret L. Induction of oxidative stress, lysosome activation and autophagy by nanoparticles in human brain-derived endothelial cells. *Biochem J*. 2012;441(3):813–821. doi:10.1042/BJ20111252
60. Leidinger P, Treptow J, Hagens K, et al. Isoniazid@Fe2 O3 nanocontainers and their antibacterial effect on tuberculosis mycobacteria. *Angew Chem Int Ed Engl*. 2015;54(43):12597–12601. doi:10.1002/anie.201505493
61. Kongseng S, Yoovathaworn K, Wongprasert K, Chunhabundit R, Sukwong P, Pissuwan D. Cytotoxic and inflammatory responses of TiO2 nanoparticles on human peripheral blood mononuclear cells. *J Appl Toxicol*. 2016;36(10):1364–1373. doi:10.1002/jat.v36.10
62. Ursini CL, Cavallo D, Fresegna AM, et al. Evaluation of cytotoxic, genotoxic and inflammatory response in human alveolar and bronchial epithelial cells exposed to titanium dioxide nanoparticles. *J Appl Toxicol*. 2014;34(11):1209–1219. doi:10.1002/jat.v34.11
63. Pan L, Lee YM, Lim TK, Lin Q, Xu X. Quantitative proteomics study reveals changes in the molecular landscape of human embryonic stem cells with impaired stem cell differentiation upon exposure to titanium dioxide nanoparticles. *Small*. 2018;14(23):e1800190. doi:10.1002/smll.v14.23
64. Kaiser JP, Roesslein M, Diener L, Wichser A, Nowack B, Wick P. Cytotoxic effects of nanosilver are highly dependent on the chloride concentration and the presence of organic compounds in the cell culture media. *J Nanobiotechnology*. 2017;15(1):5. doi:10.1186/s12951-016-0244-3
65. Senyavina NV, Gerasimenko TN, Pulkova NV, Maltseva DV. Transport and toxicity of silver nanoparticles in hepaRG cell spheroids. *Bull Exp Biol Med*. 2016;160(6):831–834. doi:10.1007/s10517-016-3321-6
66. Kettler K, Veltman K, van de Meent D, van Wezel A, Hendriks AJ. Cellular uptake of nanoparticles as determined by particle properties, experimental conditions, and cell type. *Environ Toxicol Chem*. 2014;33(3):481–492. doi:10.1002/etc.v33.3
67. Agnihotri S, Mukherji S, Mukherji S. Immobilized silver nanoparticles enhance contact killing and show highest efficacy: elucidation of the mechanism of bactericidal action of silver. *Nanoscale*. 2013;5(16):7328–7340. doi:10.1039/c3nr00024a
68. Hrkac T, Rohl C, Podschun R, et al. Huge increase of therapeutic window at a bioactive silver/titania nanocomposite coating surface compared to solution. *Mater Sci Eng C Mater Biol Appl*. 2013;33(4):2367–2375. doi:10.1016/j.msec.2013.01.069